PHOTONICS Research

MXene-based high-performance all-optical modulators for actively Q-switched pulse generation

Qing Wu,[1,2,†] Yunzheng Wang,[1,†] Weichun Huang,[1,†] Cong Wang,[1] Zheng Zheng,[2,3] Meng Zhang,[2,*] and Han Zhang[1]

[1]International Collaborative Laboratory of 2D Materials for Optoelectronics Science and Technology of Ministry of Education, College of Optoelectronic Engineering, Shenzhen University, Shenzhen 518060, China
[2]School of Electronic and Information Engineering, Beihang University, Beijing 100191, China
[3]Beijing Advanced Innovation Center for Big Data-based Precision Medicine, Beihang University, Beijing 100083, China
*Corresponding author: mengzhang10@buaa.edu.cn

Received 3 March 2020; revised 13 April 2020; accepted 28 April 2020; posted 29 April 2020 (Doc. ID 391911); published 12 June 2020

Q-switched fiber lasers are integral tools in science, industry, and medicine due to their advantages of flexibility, compactness, and reliability. All-optical strategies to generate ultrashort pulses have obtained considerable attention as they can modulate the intracavity Q factors without employing costly and complex electrically driven devices. Here, we propose a high-performance all-optical modulator for actively Q-switched pulse generation based on a microfiber knot resonator deposited with V_2CT_x MXene. Experimental results show that the obtained Q-switching pulses exhibit a wide adjustment range of repetition rate from 1 kHz to 20 kHz, a high signal-to-background contrast ratio of ~55 dB, and a narrow pulse width of 8.82 μs, indicating great potentials of providing a simple and viable solution in photonic applications. © 2020 Chinese Laser Press

https://doi.org/10.1364/PRJ.391911

1. INTRODUCTION

Q-switched pulse fiber lasers have played an important role in various applications, such as optical communications, remote sensing, material processing, and bioscience [1–4]. Different from the passive Q-switching regime that generally utilizes saturable absorbers to induce self-modulation of intracavity quality factor (Q factor), the active approach requires an externally driven device to periodically modulate the intracavity loss or the round-trip phase change of the cavity [5,6]. Therefore, the active Q-switching regime allows versatile pulse parameters (e.g., controllable pulse width and repetition rate) and the exact timing synchronization between the Q-switched pulses and externally modulated signals. It can also avoid the potential stability problems existing in most passive Q-switched cavities, e.g., low damage threshold caused by material-based saturable absorbers with a strong incident light, which promotes them for practical applications. While there are many approaches to generate actively Q-switched pulses, including bulk electro-optical [7] or acoustic-optical [8] Q-switches, they are not without limitations, such as sophisticated spatial structure, high driving voltage, and narrow operation bandwidth. In contrast, all-optical methods offer intrinsic advantages in terms of broad bandwidth operation, ease of fabrication and implementation, and low-cost [9–12], and thus have been widely deployed in a variety of applications.

In recent years, remarkable progress has been made on two-dimensional (2D) layered materials due to their extraordinary physical properties that provide exciting opportunities for diverse photonic and optoelectronic applications, such as field effect transistors, saturable absorbers, photodetectors, polarizers, and optical modulators [13–17]. Optical modulation effects in 2D materials have been widely studied as the signal processing can be fully realized in the photonic domain. All-optical modulators (AOMs) based on the photothermal effect of 2D materials (such as graphene [18], WS_2 [19], phosphorene [20], bismuthine [21], antimonene [12], and MXenes [22]) have been demonstrated to exhibit large modulation depth, broad bandwidth operation, and ease of integration for all-fiber structures. A previous report has shown an all-optical active Q-switching utilizing an antimonene-based AOM with a high modulation depth and broad operating bandwidth [12]. However, this Q-switch has its own limitations, including poor structure stability, limited tunability of repetition rate, and complexity.

AOMs based on a microfiber knot resonator (MKR) have been successfully implemented for many applications, such as optical routing and switching, demonstrating superior performances due to their prominent advantages, including flexible configurability, compact configuration, good environmental stability, and strong light–matter interaction [23–25]. The strong

evanescent field of MKR promises its efficient interaction with materials, which makes it possible to optically control the resonance by wrapping active materials. MKR devices deposited with graphene have been reported to exhibit strong phase and intensity modulation, and been applied in a fiber laser for ultrahigh repetition rate pulse generation as a high-performance all-optical switch [25,26]. Apart from graphene, MXenes (known as 2D transition metal carbides and carbonitrides) have been demonstrated to possess excellent photothermal conversion efficiency and large thermal conductivity, which could benefit to facilitate the heat generating and dissipating processes [27]. Over 100 stoichiometric compositions of MXenes have been extensively studied, providing abundant physical, photonic, and chemical properties [28,29]. Among these compositions, V_2CT_x has attracted huge interest due to its good electron and ionic conductivity and high energy density properties [30]. More importantly, recent demonstrations have proved that V_2CT_x exhibits excellent long-term stability under ambient conditions [30,31], desirable for practical applications. Therefore, it is expected that high-performance AOMs could be achieved by combining the advantages of both MXene and MKR, and further extend their application potentials in pulsed laser engineering.

Here, we present a high-performance AOM device based on a V_2CT_x MXene-deposited MKR and utilize it as an all-optical ultrafast switch to generate stable *Q*-switched pulses. The V_2CT_x MXene is fabricated by a selective etching method and deposited onto an MKR utilizing the optical deposition method. The spectral response and temperature change of MXene-deposited MKR are examined at different pump powers, showing good resonant property and photothermal response. The proposed MXene-deposited MKR device is then used to achieve all-optical modulation, including phase modulation, intensity modulation, and wavelength tuning (when inserted in a fiber laser). With the implementation of the MXene-deposited MKR device, actively *Q*-switched pulses are generated in a fiber laser, constituting 50% shorter pulse duration compared to previous reports [12].

2. PREPARATION OF MKR AND MXENE (V_2CT_x)-BASED DEVICE

A. Fabrication and Characterization of MXene (V_2CT_x)

The V_2CT_x is synthesized by selective etching of the Al element from the V_2AlC precursor. In our experiment, 2.0 g V_2AlC (200 mesh) is added into 40 mL hydrofluoric acid (HF) (30%) under continuous stirring at 35°C for 48 h. After the reaction, the mixture is diluted by a large amount of deionized water (DI H_2O), and then centrifuged for a couple of times (5000 r/min, 10 min per cycle) until the pH of the supernatant is >6. The V_2C is obtained by filtration through a polyvinylidene fluoride membrane (0.45 μm mesh) and washed with a large quantity of DI H_2O (~2 L). The procedure of the delamination of as-etched V_2AlC for V_2CT_x nanosheets is similar to that of $Ti_3C_2T_x$ nanosheets [32]. The as-obtained V_2C slurry is first dispersed into DI H_2O (~5 mg · mL^{-1}), followed by a sonication process in a water bath with a built-in water-cooling system for 8 h at 400 W. The temperature is fixed at 10°C in the whole sonication process. Afterwards, the dispersion is initially centrifuged at a speed of 5000 r/min for 30 min, and then the supernatant containing V_2CT_x nanosheets is gently decanted to another test tube and further centrifuged at a centrifugation speed of 18,000 r/min for another 30 min. The obtained precipitate is dried at 80°C in vacuum.

Figure 1 shows the characterization of the as-fabricated etched V_2C and as-exfoliated V_2CT_x nanosheets. The basal planes fan out and spread apart after HF treatment [Fig. 1(a)], indicating the successful removal of Al from V_2AlC. The transmission electron microscopy (TEM) analysis of the exfoliated nanosheets [Fig. 1(b)] presents a higher transparency of V_2CT_x nanosheets when compared with super-thin carbon membrane, indicating the nanosheets are quite thin. The lateral size range is from ~100 to ~250 nm. The crystal structure of the V_2CT_x nanosheets can be further confirmed by the high-resolution TEM (HRTEM) and selected area electron diffraction, shown in

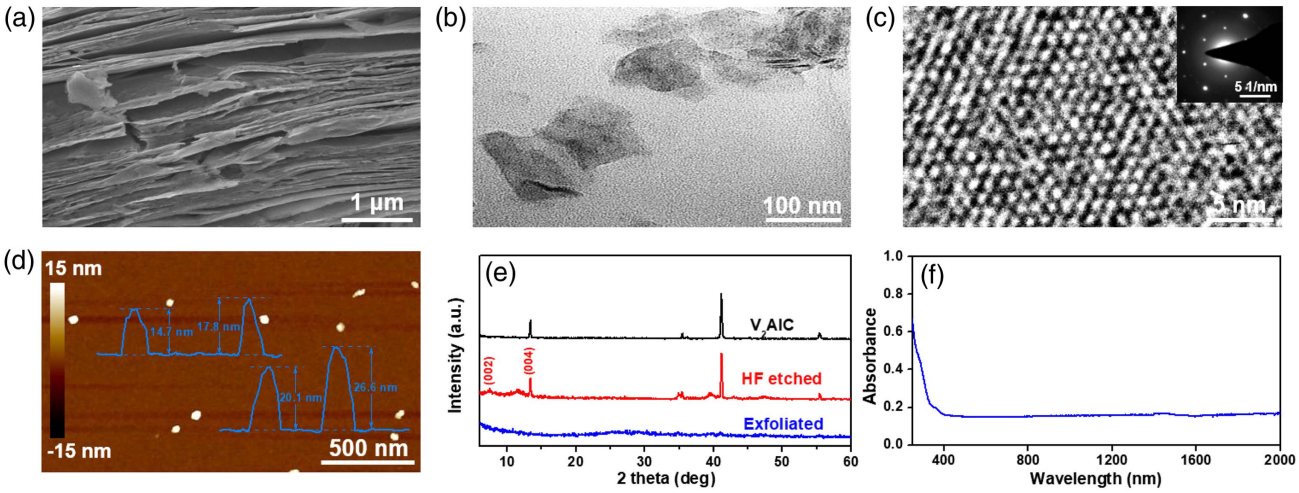

Fig. 1. Structural characterization of MXene (V_2CT_x). (a) SEM image of V_2C after selective removal of Al. (b) TEM image of exfoliated V_2CT_x nanosheets. (c) HRTEM image of exfoliated V_2CT_x nanosheets. (d) AFM image of exfoliated V_2CT_x nanosheets. (e) XRD patterns of V_2AlC, V_2C, and exfoliated V_2CT_x nanosheets. (f) UV-Vis-NIR spectrum of exfoliated V_2CT_x nanosheets.

Fig. 1(c), which is in good agreement with previous demonstrations [33]. The atomic force microscopy (AFM) is employed to determine the thickness of the V_2CT_x nanosheets, demonstrating that the thicknesses of the samples are 14.7 nm, 17.8 nm, 20.1 nm, and 26.6 nm, respectively [Fig. 1(d)]. The X-ray diffraction (XRD) patterns of V_2AlC, V_2C, and V_2CT_x nanosheets [Fig. 1(e)] indicate that after the Al-layer in V_2AlC is selectively etched in HF, the (002) peak at 8.6° in the XRD pattern of V_2C appeared, corresponding to a *c*-lattice parameter of 20.5 Å, suggesting the success of selective etching of V_2AlC. No obvious XRD signal can be observed after the exfoliation, indicating that the as-etched V_2C is exfoliated sufficiently, consistent with a previous demonstration of $Ti_3C_2T_x$ [32]. Figure 1(f) shows the absorption spectrum of the V_2CT_x nanosheets, ranging from 280 nm to 2000 nm, implying the broad bandwidth operation range of the material.

B. Fabrication and Spectral Response of MXene-Deposited MKR

The fabrication process of the MXene-deposited MKR is as follows. The microfiber is first fabricated using a flame-heated tapering technique [34], with a diameter of 3 μm, and then knotted into rings to obtain MKRs with a ring diameter of 510 μm. The insertion loss of the MKR is measured to be ~2.31 dB at 1550 nm and ~2.73 dB at 980 nm. The MXene is deposited onto the ring surface of the MKRs utilizing an optical deposition approach [35], with a deposition length of ~84 μm [Fig. 2(a) inset].

We then measure the spectral response of the bare MKR and MXene-deposited MKR with an experimental setup shown in Fig. 2(a). In the measurement, a broadband amplified spontaneous emission (ASE) source at 1550 nm is used as a seed source. Interferometric fringes in the transmission spectrum of the bare MKR have a free spectral range (FSR) of 1.02 nm, suggesting that the MKR has excellent resonant properties [Fig. 2(b)]. At a resonance wavelength of 1544.79 nm, the maximum extinction ratio (ER) is measured to be 16.06 dB and the corresponding Q factor is 19,309 [36]. Figure 2(c) shows the excellent resonant features of MKR deposited with MXene. At a resonance wavelength of 1546.65 nm, the maximum ER is 17.6 dB and the corresponding Q factor is 25,777. The increase of ER and Q factor is attributed to the change of resonant conditions due to deposition, i.e., the operation state of MKR translates from the over-coupled state to the critical-coupled state [37,38]. The FSR of MXene-deposited MKR is the same as that of the bare MKR, indicating that the ring diameter of MKR remains unchanged during the MXene deposition and MKR has certain stability [29,36].

3. MXENE-BASED MULTIFUNCTIONAL ALL-OPTICAL MODULATOR

A multifunctional all-optical modulator (AOM) system is built based on the MXene-deposited MKR to realize the phase modulation and intensity modulation. To achieve the phase modulation, a 20 mW ASE broadband light source (1550 nm) as a signal light and a 980 nm laser as the control light are coupled into the system via a 980/1550 nm wavelength-division multiplexer (WDM), shown in Fig. 3(a). The photothermal effect of MXene deposited on MKR is measured utilizing an infrared thermal imager (FLIR E60) at different powers of the control light (980 nm pump light). Figure 3(b) shows the typical thermograms of the MXene-deposited MKR at a pump power of 0 mW and 71 mW, respectively. The maximum temperature

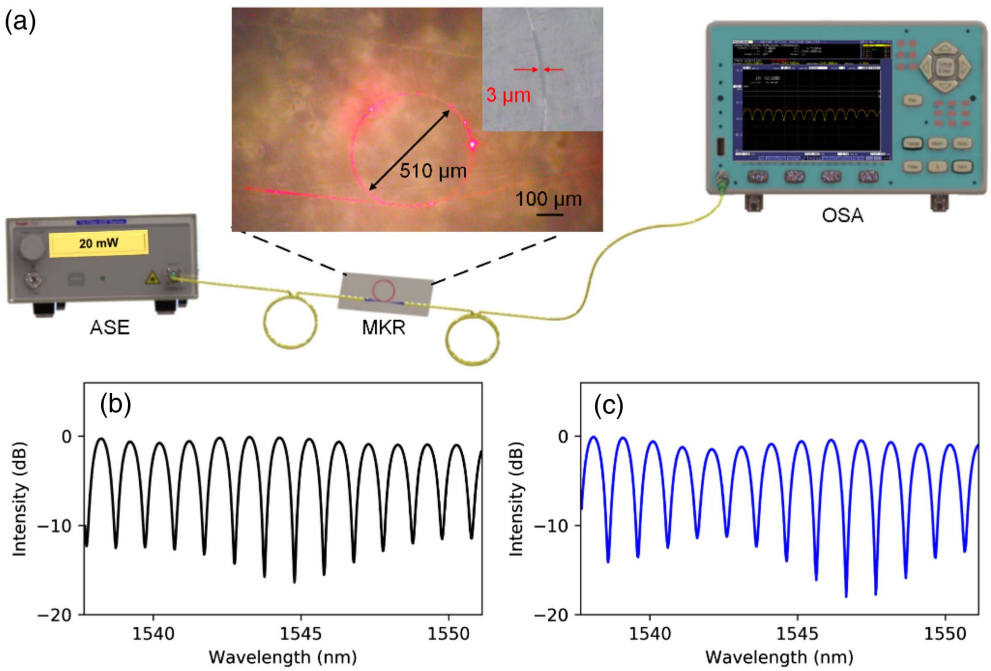

Fig. 2. (a) Experimental setup for testing the spectral response of the bare MKR and MXene-deposited MKR. Insets: optical microscopic images of MXene-deposited MKR illuminated by a red laser and a close-up of MXene-deposited MKR (inset). Transmission spectra of (b) the bare MKR and (c) the MXene-deposited MKR.

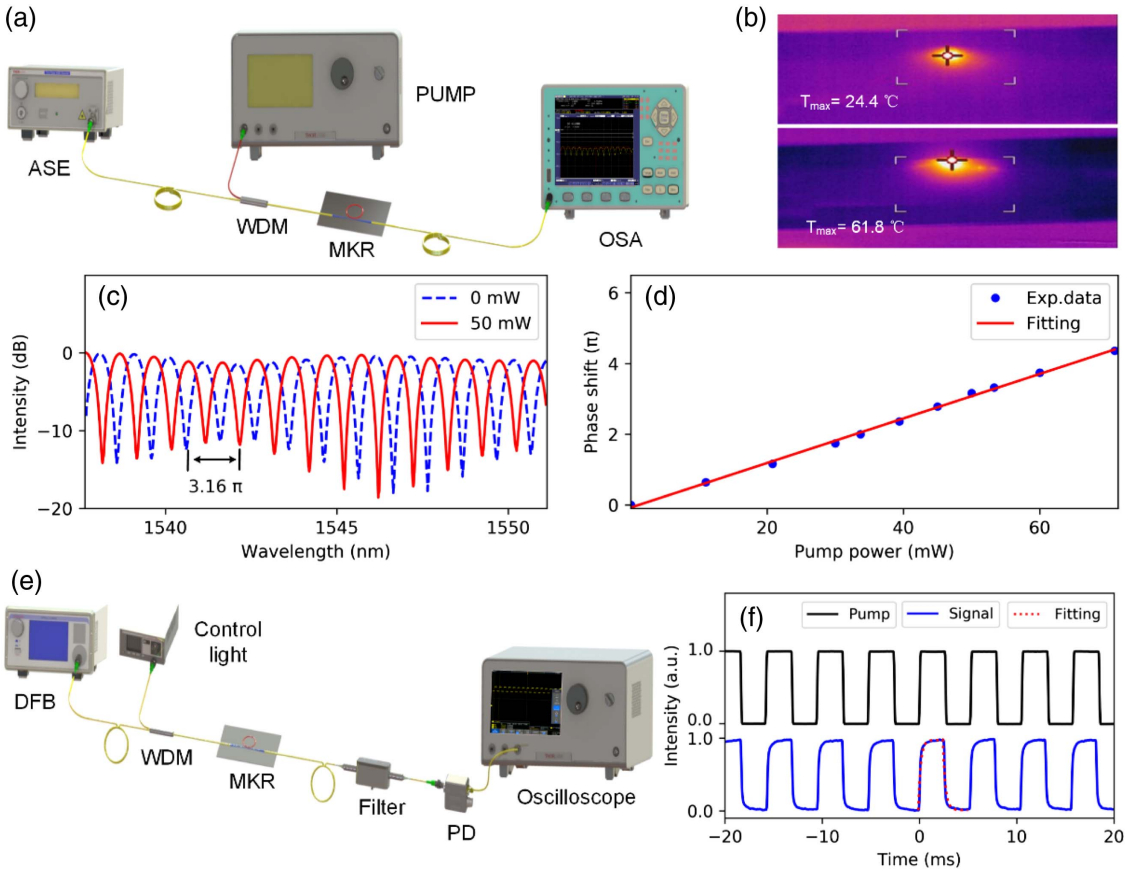

Fig. 3. (a) Experimental configuration of all-optical phase modulator based on the MXene-deposited MKR. (b) Thermograms of MXene-deposited MKR under pump power of 0 mW (upper) and 71 mW (lower). (c) Normalized transmission spectrum under pump power of 0 mW (blue dashed line) and 50 mW (red solid line). (d) Phase shift versus pump power. (e) Experimental configuration of all-optical intensity modulator based on the MXene-deposited MKR. (f) Waveforms of input pump light (black solid line), output signal light (blue solid line), and its fitting curves (red dotted line).

is measured to be 61.8°C at 71 mW and 24.4°C at 0 mW, corresponding to a temperature rise of 37.4°C. The measurement is carried out under the same condition when using a bare MKR. However, no significant temperature rise can be observed, indicating the good photothermal conversion property of MXene.

The normalized transmission spectra of signal light at different pump powers are shown in Fig. 3(c), where a blue dashed line refers to a pump power of 0 mW and a red solid line refers to 50 mW. We observe that the resonant peaks shift to the long wavelength direction when the pump power increases as the large amount of heat induced by the strong photothermal effect of MXene changes the refractive index of both MXene and MKR, so that the optical phase and resonant conditions of the signal light are changed accordingly. At a pump power of 50 mW, the wavelength shift is measured to be 1.61 nm, corresponding to the phase shift of 3.16π. The phase shift as a function of pump power is presented in Fig. 3(d), demonstrating a linear relationship with a conversion efficiency of $0.063\pi/\text{mW}$. It is noted that the proposed MKR-based AOM has a larger conversion efficiency compared with AOMs based on a Mach–Zehnder interferometer [22] or a Michelson interferometer [21], due to the longer light–matter interaction length in the microfiber device.

To achieve the intensity modulation, the signal source is replaced by a narrow-bandwidth continuous-wave distributed feedback laser [Fig. 3(e)]. The pump light is modulated to a square wave with a frequency of 188 Hz and a duty cycle of 50% by a control unit [black solid line in Fig. 3(f)]. The residual 980 nm light is extracted by a bandpass filter to ensure no pump light exists at the output port. A typical output signal waveform is shown in Fig. 3(f), blue traces representing the output signal waveform. It is clearly seen that the output signal light has the same frequency and duty cycle as the input square wave pump light, indicating that the signal light has been successfully modulated. The rising and falling edges of the output signal light are smoother than those of the input pump light, mainly resulting from the slow response of the heat generation and dissipation. By fitting the edges of the output signal light waveform with exponential functions [red dotted curves in Fig. 3(f)], the rising and falling time constants are evaluated to be 238 μs and 265 μs, respectively, much shorter than the previous demonstrations in Refs. [21,22] due to the small microfiber diameter enhancing the light–matter interaction and

the excellent thermal conductivity of MXene. The modulation depth of the intensity modulation at 1550 nm is estimated to be ~12.7 dB [Fig. 3(c)].

The variable transmission spectrum property of the MXene-deposited MKR-based AOM indicates that this device can be used in a fiber laser as a tunable filter (TF). The experimental setup of the tunable fiber laser is shown in Fig. 4(a), consisting of a 0.98 m Er-doped fiber (YOFC, EDF80) as the gain medium, co-pumped by a 980 nm pump light from PUMP1 through the WDM1, a 90:10 optical coupler for spectral and time diagnostics, and a polarization-independent optical isolator to ensure unidirectional propagation. The spectral property of the MXene-deposited-MKR is modulated by PUMP2 (980 nm). The total cavity length is ~22 m.

The fiber laser operates in the continuous-wave regime. When PUMP1 was set to be 34 mW, Fig. 4(b) shows the output spectrum centered at 1555.91 nm with a full width at half-maximum (FWHM) spectral bandwidth of 0.05 nm and a signal-to-background contrast ratio of >50 dB, indicating good operation. The spikes of the output spectrum are due to the quasi-periodic characteristics of transmission of AOM, with the peak interval of 1.02 nm equivalent to the FSR. When PUMP2 is increased from 0 mW to 22 mW, the output wavelength is tunable from 1555.9 nm to 1556.76 nm, showing a slope of 0.039 nm/mW against the PUMP2 power based on a linear fit [Figs. 4(c) and 4(d)]. When PUMP2 is set to 33 mW, dual-wavelength operation can be observed in the cavity, shown in Fig. 4(e), with a measured peak interval of

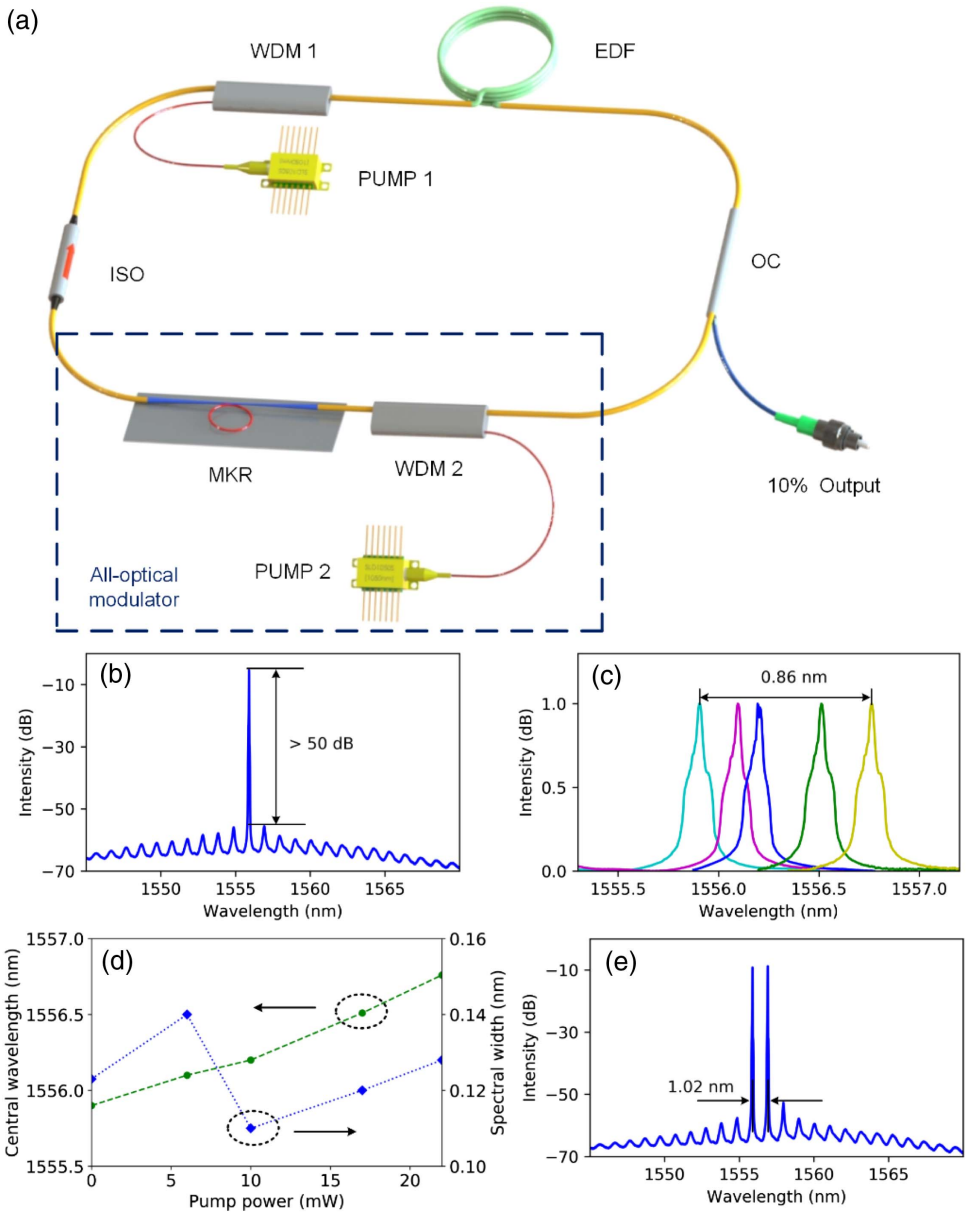

Fig. 4. (a) Experimental setup of the wavelength tunable fiber laser enabled by the proposed AOM. (b) Typical laser spectrum at PUMP1 power of 34 mW. (c) The laser spectra at different PUMP2 powers (0 mW, 6 mW, 10 mW, 17 mW, and 22 mW). (d) Dependence of central wavelength and spectral width on PUMP2 power. (e) The laser spectrum at PUMP2 power of 33 mW.

1.02 nm which is equal to the FSR of AOM. This dual-wavelength emission is attributed to the erbium gain spectral property, cavity loss, and transmission of the AOM [26].

4. ALL-OPTICAL ACTIVE Q-SWITCH

The demonstrated intensity and phase modulation property of the MXene-based AOM at 1550 nm indicates that the device could be used to modulate the loss and Q factor of an erbium-doped fiber laser cavity. This could in turn be deployed to generate a regular train of actively Q-switched pulses in this spectral region. Figure 5(a) shows the configuration of the cavity, with a total cavity length of ~22.5 m and 0.98 m erbium-doped fiber (YOFC, EDF80). A TF with a 0.05 nm spectral width (following Ref. [12], the passband needs to be smaller than the FSR of the modulator) is included in the laser cavity. The cavity produces continuous wave when only PUMP1 is on. When PUMP2 is set to be 58 mW, the output is modulated to a pulse with a frequency of 17.37 kHz and a duty cycle of 1:1. When the peak of transmission of the all-optical modulator is located within the passband of the TF, the cavity loss is low and thus the Q factor is high. When the bottom of the transmission is within the bandpass of the TF, the cavity loss is large and the corresponding Q value is low. This means that the intracavity loss switching is achieved by the combination of the transmission of the modulator (through pump power adjustment) and the TF. The obtained Q-switched pulses have a repetition rate of 17.37 kHz, synchronized with PUMP2 pulses. The cavity repetition rate can be tuned from 1 kHz to 20 kHz by changing the frequency of PUMP2.

Typical output characteristics of the laser are shown in Figs. 5(b)–5(d). Pulses are generated with 56 μs spacing, corresponding to 17.73 kHz repetition rate [Fig. 5(b)] and FWHM pulse duration of 8.82 μs [Fig. 5(c)]. The corresponding spectrum has an FWHM spectral bandwidth of 0.016 nm, centered at 1565.12 nm [Fig. 5(d)]. The signal-to-background ratio is 54.63 dB, indicating that the actively Q-switched fiber laser operates in low noise.

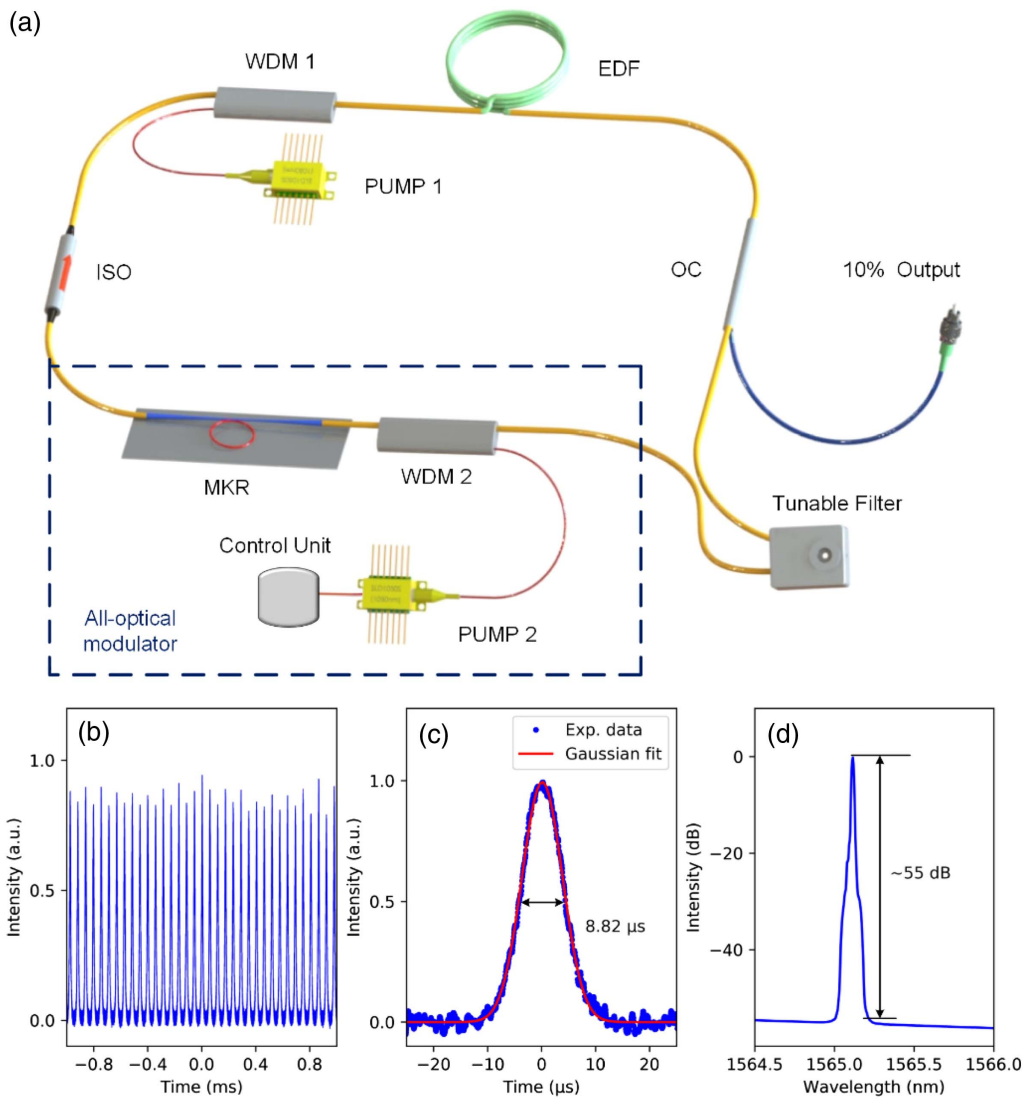

Fig. 5. (a) Schematic diagram of the actively Q-switched fiber laser enabled by the proposed AOM. (b) Waveforms of active Q-switching pulse trains. (c) Single pulse profile fitted by a Gaussian function. (d) Laser spectrum.

5. CONCLUSION

In summary, we have demonstrated a multifunctional high-performance all-optical modulator based on a MXene-deposited MKR and applied it to an actively *Q*-switched Er-doped fiber laser, for the first time. This laser delivers stable pulses with a wide frequency range from 1 kHz to 20 kHz, a high signal-to-noise ratio of 54.63 dB, and a narrow pulse width of 8.82 μs. Compared to previous demonstrations utilizing MKR-based modulators deposited with two-dimensional layered materials, our results represent the shortest pulse duration achieved from an MKR deposited with a narrow spectral width and wide adjustment range of cavity repetition rate. Our simple design and fabrication strategy promote the development of novel 2D material-based all-optical devices in fiber laser technology.

Funding. National Natural Science Foundation of China (51778030, 51978024, 61435010, 61875138, 61961136001); State Key Research Development Program of China (2019YFB2203503); Science, Technology and Innovation Commission of Shenzhen Municipality (GJHZ20180928160209731, JCYJ20170811093453105, JCYJ20180307164612205, KQTD2015032416270385).

Acknowledgment. The authors also acknowledge the support from Instrumental Analysis Center of Shenzhen University (Xili Campus).

Disclosures. The authors declare that they have no conflicts of interest related to this work.

[†]These authors contributed equally to this work.

REFERENCES

1. R. I. Woodward, M. R. Majewski, N. Macadam, G. Hu, T. Albrow-Owen, T. Hasan, and S. D. Jackson, "*Q*-switched Dy:ZBLAN fiber lasers beyond 3 μm: comparison of pulse generation using acousto-optic modulation and inkjet-printed black phosphorus," Opt. Express **27**, 15032–15045 (2019).
2. J. Alaniz-Baylon, M. Duran-Sanchez, R. I. Alvarez-Tamayo, B. Posada-Ramirez, M. Bello-Jimenez, B. Ibarra-Escamilla, A. A. Castillo-Guzman, and E. A. Kuzin, "Fiber laser with simultaneous multi-wavelength Er/Yb passively *Q*-switched and single-wavelength Tm gain-switched operations," Photon. Res. **7**, 608–614 (2019).
3. K. Wu, X. Zhang, J. Wang, X. Li, and J. Chen, "WS_2 as a saturable absorber for ultrafast photonic applications of mode-locked and *Q*-switched lasers," Opt. Express **23**, 11453–11461 (2015).
4. M. Zhang, G. H. Hu, G. Q. Hu, R. C. T. Howe, L. Chen, Z. Zheng, and T. Hasan, "Yb- and Er-doped fiber laser *Q*-switched with an optically uniform, broadband WS_2 saturable absorber," Sci. Rep. **5**, 17482 (2015).
5. L. Escalante-Zarate, Y. O. Barmenkov, J. L. Cruz, and M. V. Andres, "*Q*-switch modulator as a pulse shaper in *Q*-switched fiber lasers," IEEE Photonics Technol. Lett. **24**, 312–314 (2012).
6. T. Hu, D. D. Hudson, and S. D. Jackson, "Actively *Q*-switched 2.9 μm $Ho^{3+}Pr^{3+}$-doped fluoride fiber laser," Opt. Lett. **37**, 2145–2147 (2012).
7. H. H. Kee, G. P. Lee, and T. P. Newson, "Narrow linewidth CW and *Q*-switched erbium-doped fibre loop laser," Electron. Lett. **34**, 1318–1319 (1998).
8. J. A. Alvarez-Chavez, H. L. Offerhaus, J. Nilsson, P. W. Turner, W. A. Clarkson, and D. J. Richardson, "High-energy, high-power ytterbium-doped *Q*-switched fiber laser," Opt. Lett. **25**, 37–39 (2000).
9. R. J. Williams, N. Jovanovic, G. D. Marshall, and M. J. Withford, "All-optical, actively *Q*-switched fiber laser," Opt. Express **18**, 7714–7723 (2010).
10. H. G. Yun, S. H. Lee, M. H. Lee, and K. H. Kim, "An actively *Q*-switched single-longitudinal-mode fiber laser with an optically pumped saturable absorber," Laser Phys. **23**, 095107 (2013).
11. A. B. Ren, M. Feng, F. Song, Y. Y. Ren, S. Yang, Z. G. Yang, Y. G. Li, Z. B. Liu, and J. G. Tian, "Actively *Q*-switched ytterbium-doped fiber laser by an all-optical *Q*-switcher based on graphene saturable absorber," Opt. Express **23**, 21490–21496 (2015).
12. Y. Z. Wang, W. C. Huang, C. Wang, J. Guo, F. Zhang, Y. F. Song, Y. Q. Ge, L. M. Wu, J. Liu, J. Q. Li, and H. Zhang, "An all-optical, actively *Q*-switched fiber laser by an antimonene-based optical modulator," Laser Photonics Rev. **13**, 1800313 (2019).
13. M. Zhang, Q. Wu, F. Zhang, L. L. Chen, X. X. Jin, Y. W. Hu, Z. Zheng, and H. Zhang, "2D black phosphorus saturable absorbers for ultrafast photonics," Adv. Opt. Mater. **7**, 1800224 (2019).
14. Z. P. Sun, A. Martinez, and F. Wang, "Optical modulators with 2D layered materials," Nat. Photonics **10**, 227–238 (2016).
15. G. Hu, T. Albrow-Owen, X. Jin, A. Ali, Y. Hu, R. C. T. Howe, K. Shehzad, Z. Yang, X. Zhu, R. I. Woodward, T.-C. Wu, H. Jussila, J.-B. Wu, P. Peng, P.-H. Tan, Z. Sun, E. J. R. Kelleher, M. Zhang, Y. Xu, and T. Hasan, "Black phosphorus ink formulation for inkjet printing of optoelectronics and photonics," Nat. Commun. **8**, 278 (2017).
16. Q. Wu, X. Jin, S. Chen, X. Jiang, Y. Hu, Q. Jiang, L. Wu, J. Li, Z. Zheng, M. Zhang, and H. Zhang, "MXene-based saturable absorber for femtosecond mode-locked fiber lasers," Opt. Express **27**, 10159–10170 (2019).
17. X. Jin, G. Hu, M. Zhang, Y. Hu, T. Albrow-Owen, R. C. T. Howe, T.-C. Wu, Q. Wu, Z. Zheng, and T. Hasan, "102 fs pulse generation from a long-term stable, inkjet-printed black phosphorus-mode-locked fiber laser," Opt. Express **26**, 12506–12513 (2018).
18. X. T. Gan, C. Y. Zhao, Y. D. Wang, D. Mao, L. Fang, L. Han, and J. L. Zhao, "Graphene-assisted all-fiber phase shifter and switching," Optica **2**, 468–471 (2015).
19. K. Wu, C. S. Guo, H. Wang, X. Y. Zhang, J. Wang, and J. P. Chen, "All-optical phase shifter and switch near 1550 nm using tungsten disulfide (WS_2) deposited tapered fiber," Opt. Express **25**, 17639–17649 (2017).
20. Y. Z. Wang, F. Zhang, X. Tang, X. Chen, Y. X. Chen, W. C. Huang, Z. M. Liang, L. M. Wu, Y. Q. Ge, Y. F. Song, J. Liu, D. Zhang, J. Q. Li, and H. Zhang, "All-optical phosphorene phase modulator with enhanced stability under ambient conditions," Laser Photonics Rev. **12**, 1800016 (2018).
21. Y. Z. Wang, W. C. Huang, J. L. Zhao, H. Huang, C. Wang, F. Zhang, J. Liu, J. Q. Li, M. Zhang, and H. Zhang, "A bismuthene-based multi-functional all-optical phase and intensity modulator enabled by photothermal effect," J. Mater. Chem. C **7**, 871–878 (2019).
22. Q. Wu, S. Chen, Y. Z. Wang, L. M. Wu, X. T. Jiang, F. Zhang, X. X. Jin, Q. Y. Jiang, Z. Zheng, J. Q. Li, M. Zhang, and H. Zhang, "MZI-based all-optical modulator using MXene $Ti_3C_2T_x$ (T = F, O, or OH) deposited microfiber," Adv. Mater. Technol. **4**, 1800532 (2019).
23. Y. Xie, D. Cai, H. Wu, J. Pan, N. Zhou, C. Xin, S. Yu, P. Wang, X. Jiang, J. Qiu, X. Guo, and L. Tong, "Mid-infrared chalcogenide microfiber knot resonators," Photon. Res. **8**, 616–621 (2020).
24. G. W. Chen, Z. J. Zhang, X. L. Wang, H. G. Li, M. J. Jiang, H. Y. Guan, W. T. Qiu, H. H. Lu, J. L. Dong, W. G. Zhu, J. H. Yu, Y. C. Zhong, Y. H. Luo, J. Zhang, and Z. Chen, "Highly sensitive all-optical control of light in WS_2 coated microfiber knot resonator," Opt. Express **26**, 27650–27658 (2018).
25. H. H. Lu, Z. M. Wang, Z. J. Huang, J. Tao, H. Q. Xiong, W. T. Qiu, H. Y. Guan, H. Z. Dong, J. L. Dong, W. G. Zhu, J. H. Yu, Y. C. Zhong, Y. H. Luo, J. Zhang, and Z. Chen, "Resonance-assisted light-control characteristics of SnS_2 on a microfiber knot resonator with fast response," Photon. Res. **6**, 1137–1143 (2018).
26. M. Liu, R. Tang, A.-P. Luo, W.-C. Xu, and Z.-C. Luo, "Graphene-decorated microfiber knot as a broadband resonator for ultrahigh repetition-rate pulse fiber lasers," Photon. Res. **6**, C1–C7 (2018).

27. J. C. Lei, X. Zhang, and Z. Zhou, "Recent advances in MXene: preparation, properties, and applications," Front. Phys. **10**, 276–286 (2015).
28. Y. Gogotsi and B. Anasori, "The rise of MXenes," ACS Nano **13**, 8491–8494 (2019).
29. J. Li, Z. Zhang, L. Du, L. Miao, J. Yi, B. Huang, Y. Zou, C. Zhao, and S. Wen, "Highly stable femtosecond pulse generation from a MXene Ti_3C_2Tx (T = F, O, or OH) mode-locked fiber laser," Photon. Res. **7**, 260–264 (2019).
30. R. Thakur, A. VahidMohammadi, J. Moncada, W. R. Adams, M. Y. Chi, B. Tatarchuk, M. Beidaghi, and C. A. Carrero, "Insights into the thermal and chemical stability of multilayered V_2CT_x MXene," Nanoscale **11**, 10716–10726 (2019).
31. J. Chen, K. Chen, D. Y. Tong, Y. J. Huang, J. W. Zhang, J. M. Xue, Q. Huang, and T. Chen, "CO_2 and temperature dual responsive 'smart' MXene phases," Chem. Commun. **51**, 314–317 (2015).
32. M. Naguib, M. Kurtoglu, V. Presser, J. Lu, J. Niu, M. Heon, L. Hultman, Y. Gogotsi, and M. W. Barsoum, "Two-dimensional nanocrystals produced by exfoliation of Ti_3AlC_2," Adv. Mater. **23**, 4248–4253 (2011).
33. M. Naguib, J. Halim, J. Lu, K. M. Cook, L. Hultman, Y. Gogotsi, and M. W. Barsoum, "New two-dimensional niobium and vanadium carbides as promising materials for Li-ion batteries," J. Am. Chem. Soc. **135**, 15966–15969 (2013).
34. L. T. Gai, J. Li, and Y. Zhao, "Preparation and application of microfiber resonant ring sensors: a review," Opt. Laser Technol. **89**, 126–136 (2017).
35. K. Kashiwagi and S. Yamashita, "Deposition of carbon nanotubes around microfiber via evanascent light," Opt. Express **17**, 18364–18370 (2009).
36. X. S. Jiang, L. M. Tong, G. Vienne, X. Guo, A. Tsao, Q. Yang, and D. R. Yang, "Demonstration of optical microfiber knot resonators," Appl. Phys. Lett. **88**, 223501 (2006).
37. A. Yariv, "Critical coupling and its control in optical waveguide-ring resonator systems," IEEE Photonics Technol. Lett. **14**, 483–485 (2002).
38. C. Y. Qiu, Y. X. Yang, C. Li, Y. F. Wang, K. Wu, and J. P. Chen, "All-optical control of light on a graphene-on-silicon nitride chip using thermo-optic effect," Sci. Rep. **7**, 17046 (2017).